Electronic Supplementary Material (ESI) for Nanoscale.

High-yield halide-assisted synthesis of metal-organic framework UiO-based nanocarriers

Manuel Ceballos,[a] Manuela Cedrún-Morales,[a] Manuel Rodríguez-Pérez,[b] Samuel Funes-Hernando,[b] José Manuel Vila-Fungueiriño,[b] Giulia Zampini,[b] Maria F. Navarro Poupard,[b] Ester Polo,[c] Pablo del Pino*[a] and Beatriz Pelaz.*[d]

[a] Centro Singular de Investigación en Química Biolóxica e Materiais Moleculares (CiQUS), Departamento de Física de Partículas, Universidade de Santiago de Compostela, 15782 Santiago de Compostela, Spain.
[b] Centro Singular de Investigación en Química Biolóxica e Materiais Moleculares (CiQUS), Universidade de Santiago de Compostela, 15782 Santiago de Compostela, Spain.
[c] Centro Singular de Investigación en Química Biolóxica e Materiais Moleculares (CiQUS), Departamento de Bioquímica y Biología Molecular, Universidade de Santiago de Compostela, 15782 Santiago de Compostela, Spain.
[d] Centro Singular de Investigación en Química Biolóxica e Materiais Moleculares (CiQUS), Departamento de Química Inorgánica, Universidade de Santiago de Compostela, 15782 Santiago de Compostela, Spain.

SUPPORTING INFORMATION

S1. Influence of modulator, Zr precursor and halide

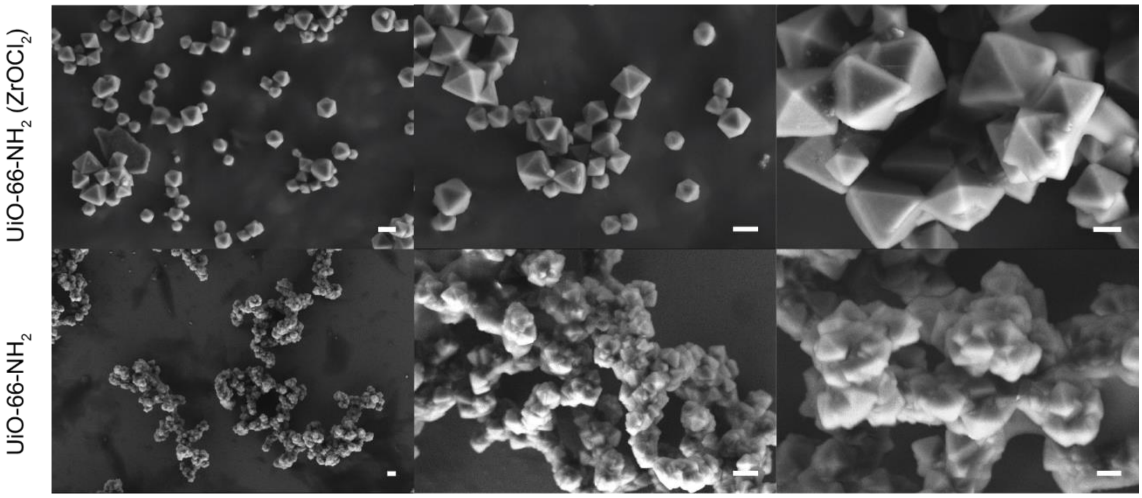

Figure S1. Representative SEM images of UiO-66-NH$_2$ (ZrOCl$_2$) and UiO-66-NH$_2$ particles obtained using different Zr precursors. Images were taken at different magnifications collected with Everhart-Thornley detector (SE2, secondary electrons) at 3 kV as well as different voltages to get different information. Scale bars from left to right correspond to 500 nm, 400 nm and 200 nm.

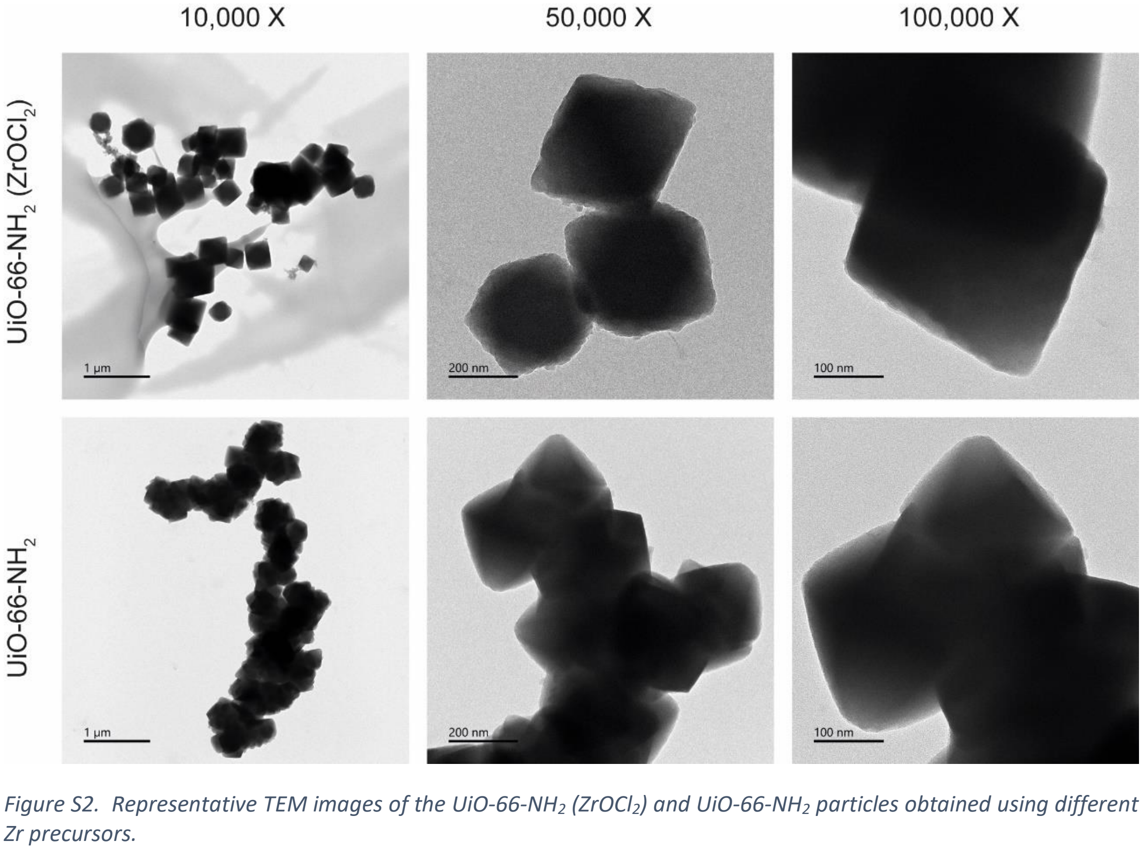

Figure S2. Representative TEM images of the UiO-66-NH$_2$ (ZrOCl$_2$) and UiO-66-NH$_2$ particles obtained using different Zr precursors.

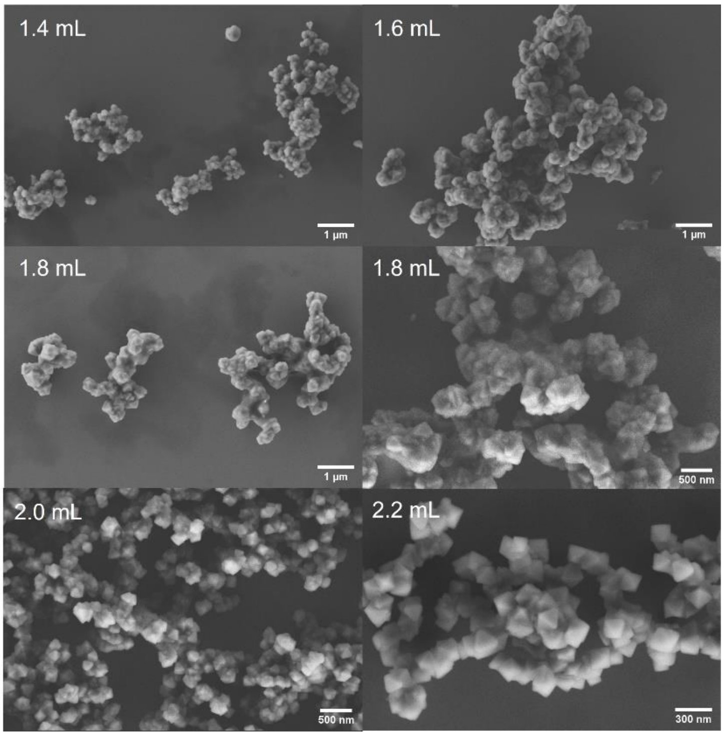

Figure S3. UiO-66-NH_2 particles synthesized with $ZrO(NO_3)_2$ as precursor with different amounts of acetic acid as modulator 1.4, 1.6, 1.8, 2.0 and 2.2 mL (775, 885, 995, 1105, 1215 equivalents). Images were taken at different magnifications collected with Everhart-Thornley detector (SE2, secondary electrons) at 3 kV as well as different voltages to get different information.

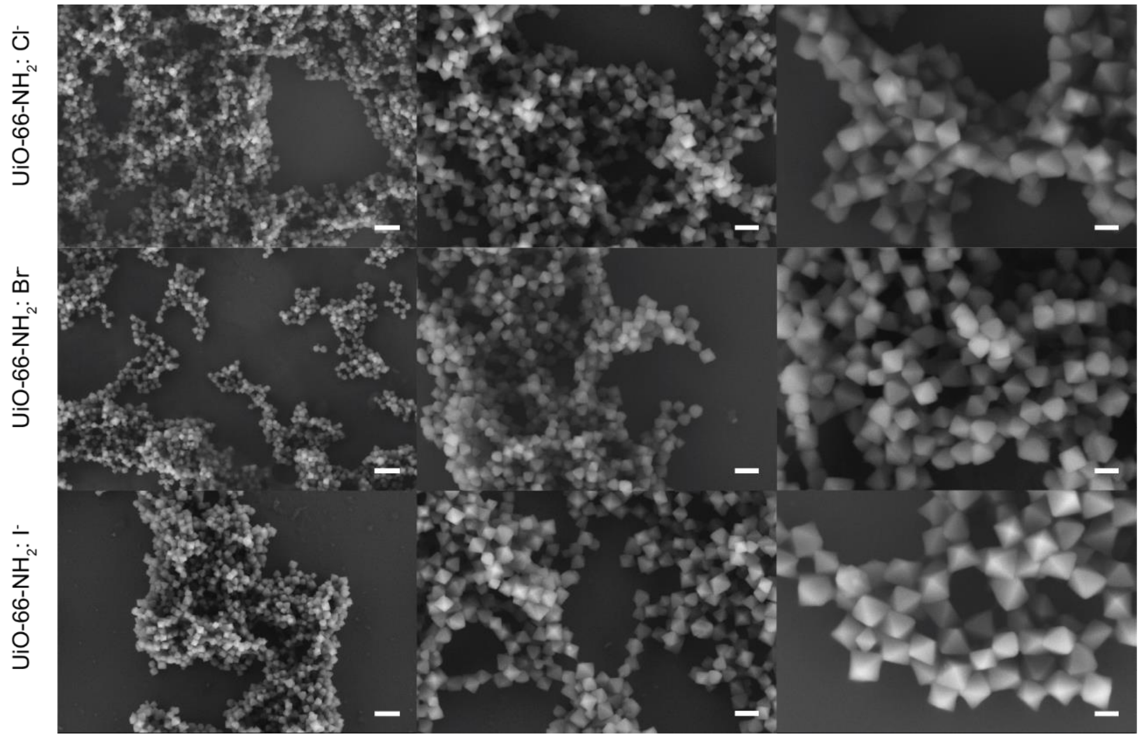

Figure S4. Representative SEM images of UiO-66-NH_2:X^- (X^-: Cl^-, Br^-, I^-) NMOFs at different magnifications collected with Everhart-Thornley detector (SE2, secondary electrons) at 3 kV as well as different voltages to get different information. Scale bars from left to right correspond to 400nm, 200 nm and 100 nm.

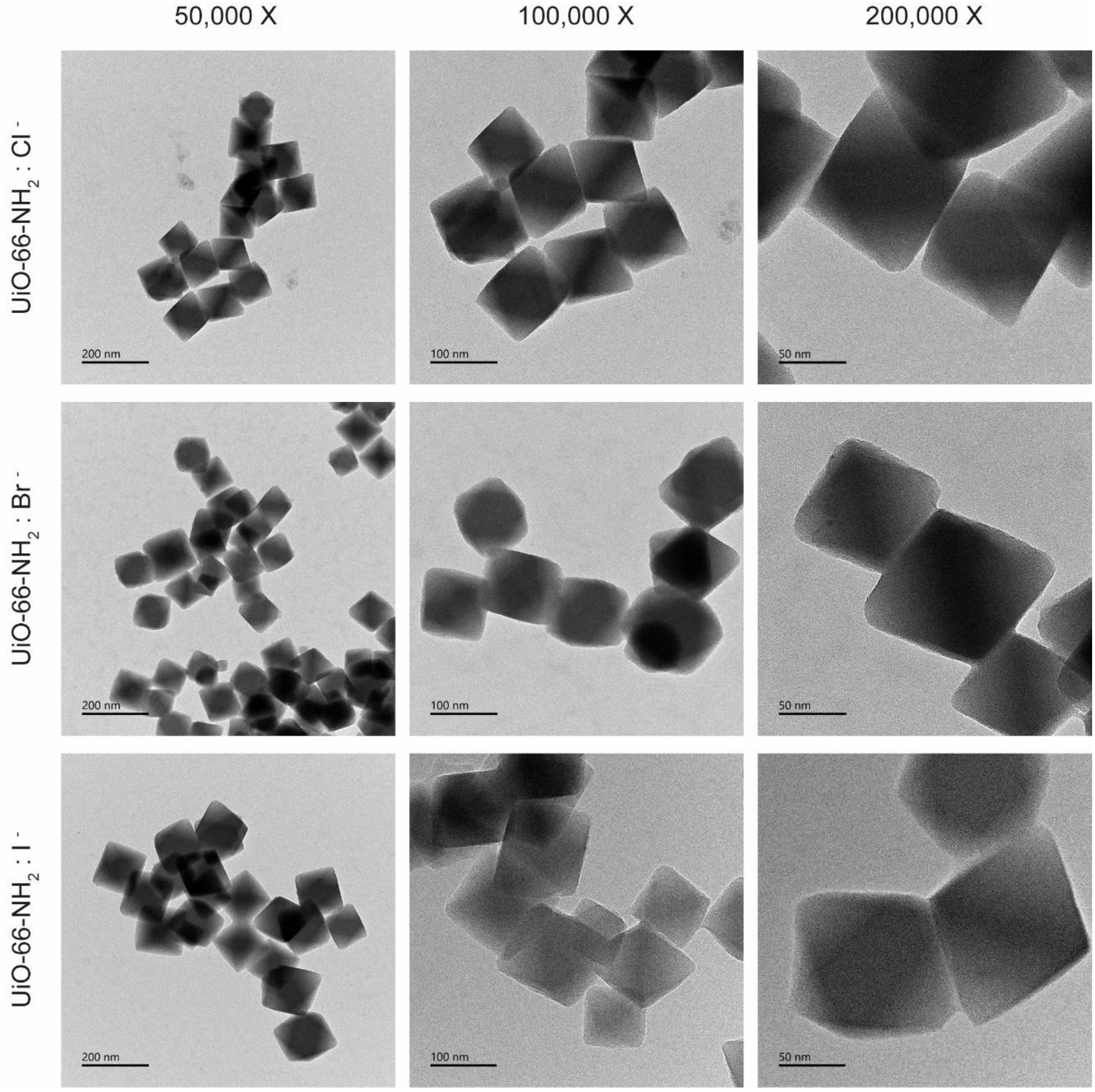

Figure S5. Representative TEM images of UiO-66-NH$_2$:X$^-$ (X$^-$: Cl$^-$, Br$^-$, I$^-$) NMOFs.

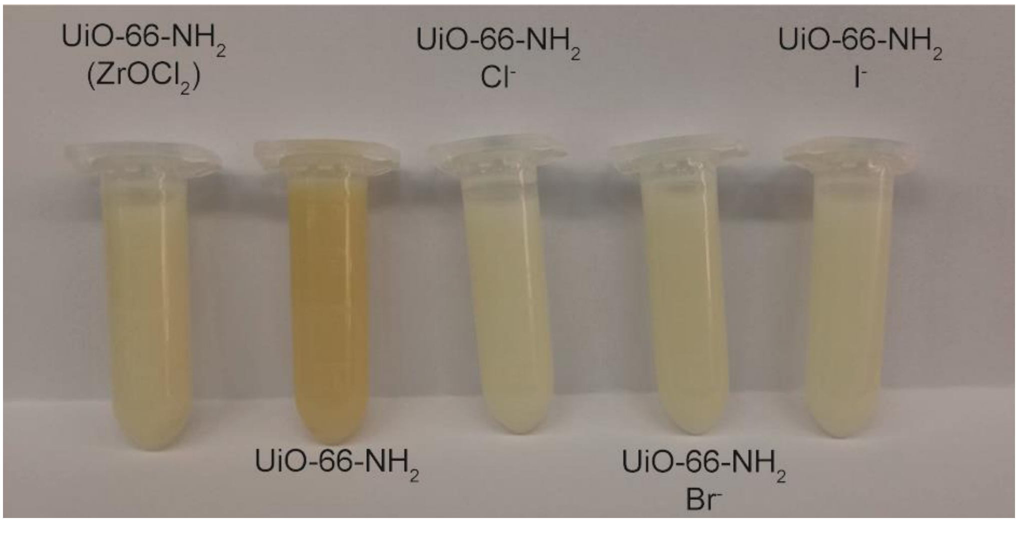

Figure S6. Photograph of the different UiO-66-NH$_2$ particles produced dispersed in methanol.

The histograms of the number distribution (the edge length of particles from the SEM images) are presented in Figure S7. The size of the particles was also corroborated with NTA and DLS measurements, results are summarized in Table S5.

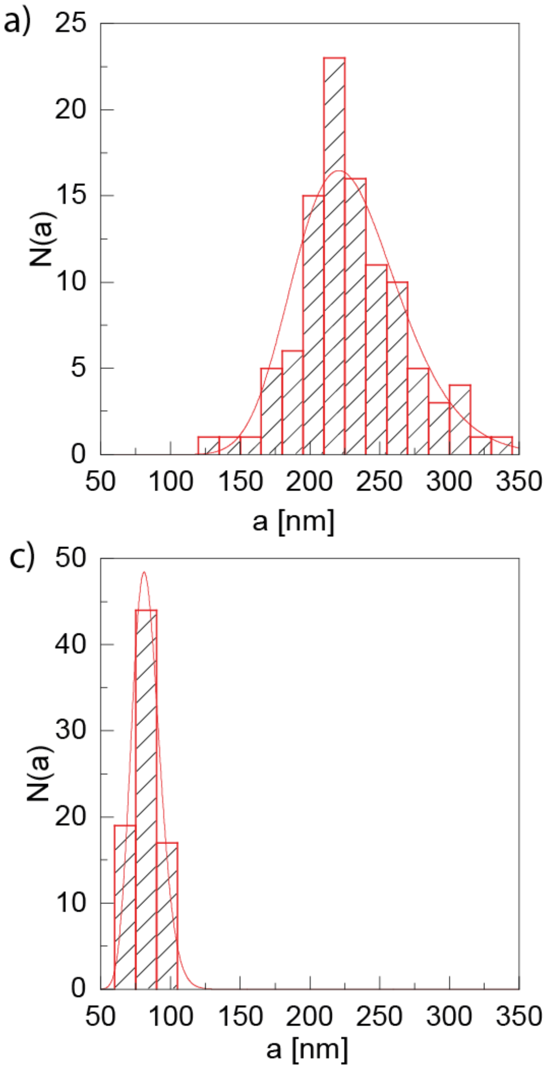

Figure S7. Histogram of the number distribution N of the edge of the nanoparticles (i.e., vertex-to vertex distance) as determined from SEM images. a) UiO-66-NH$_2$ (ZrOCl$_2$) 225 ± 37 nm, b) UiO-66-NH$_2$:Cl$^-$ 94 ± 10 nm, c) UiO-66-NH$_2$:Br$^-$ 81 ± 9 nm and d) UiO-66-NH$_2$:I$^-$ 109 ± 14 nm.

Influence of the different halides as co-modulator during the formation of the Zr-cluster.

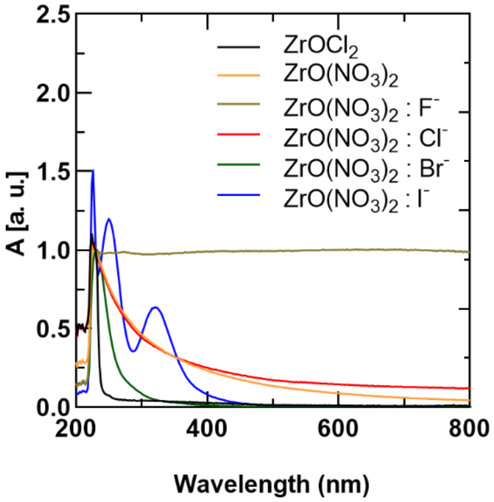

Figure S8. UV-VIS absorption spectra of the zirconium precursors $ZrClO_2$ and $ZrO(NO_3)_2$ and the effect of halides with $ZrO(NO_3)_2$ in DMF solution.

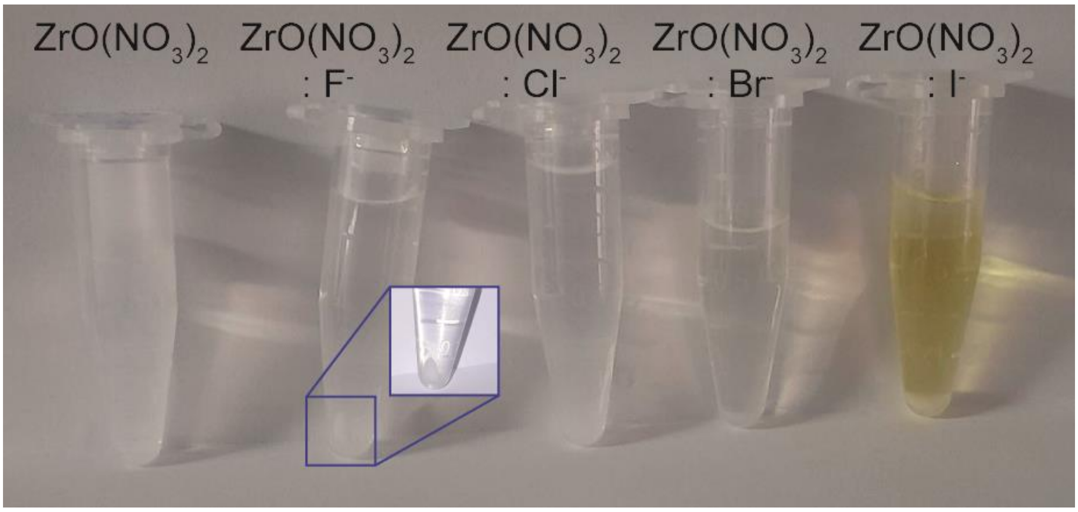

Figure S9. $ZrO(NO_3)_2$ solutions in presence of sodium halide salts in DMF. In the case of F^- the formation of a white precipitate was observed (inset).

S2. UiO-NH_2 NMOFs characterization

General Considerations

Figure S10 shows the unit cell represented using Mercury 2020.3.0 with the .cif file published by Christopher A. Trickett *et al.* [1] The reported data of the size of the unit cell (Table S1) combined with both Zr concentration (mg Zr/mL) and NMOFs´ volume, allowed us to calculate the molar (nM) concentration (see ICP-OES section).

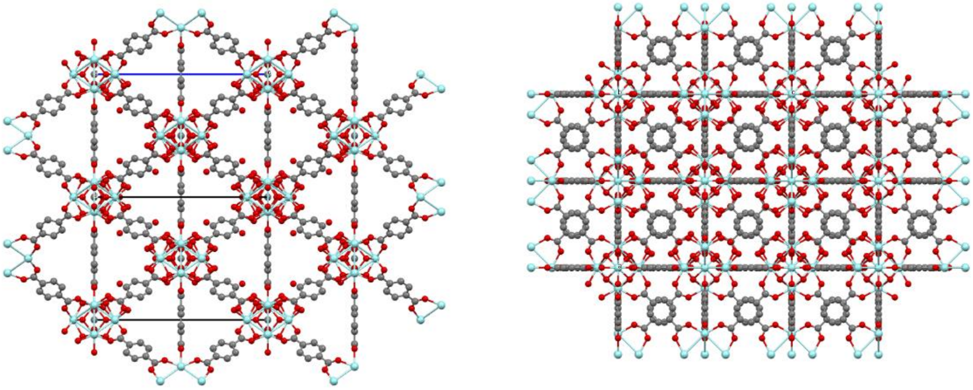

Figure S10: Mercury images of the unit cell of UiO-66.

a unit cell (nm)	2.1
V unit cell nm^3	8.9
Zr in a unit cell	24.0
MW Zr (g/mol)	91.2

Table S1. Unit cell parameters of UiO-66.

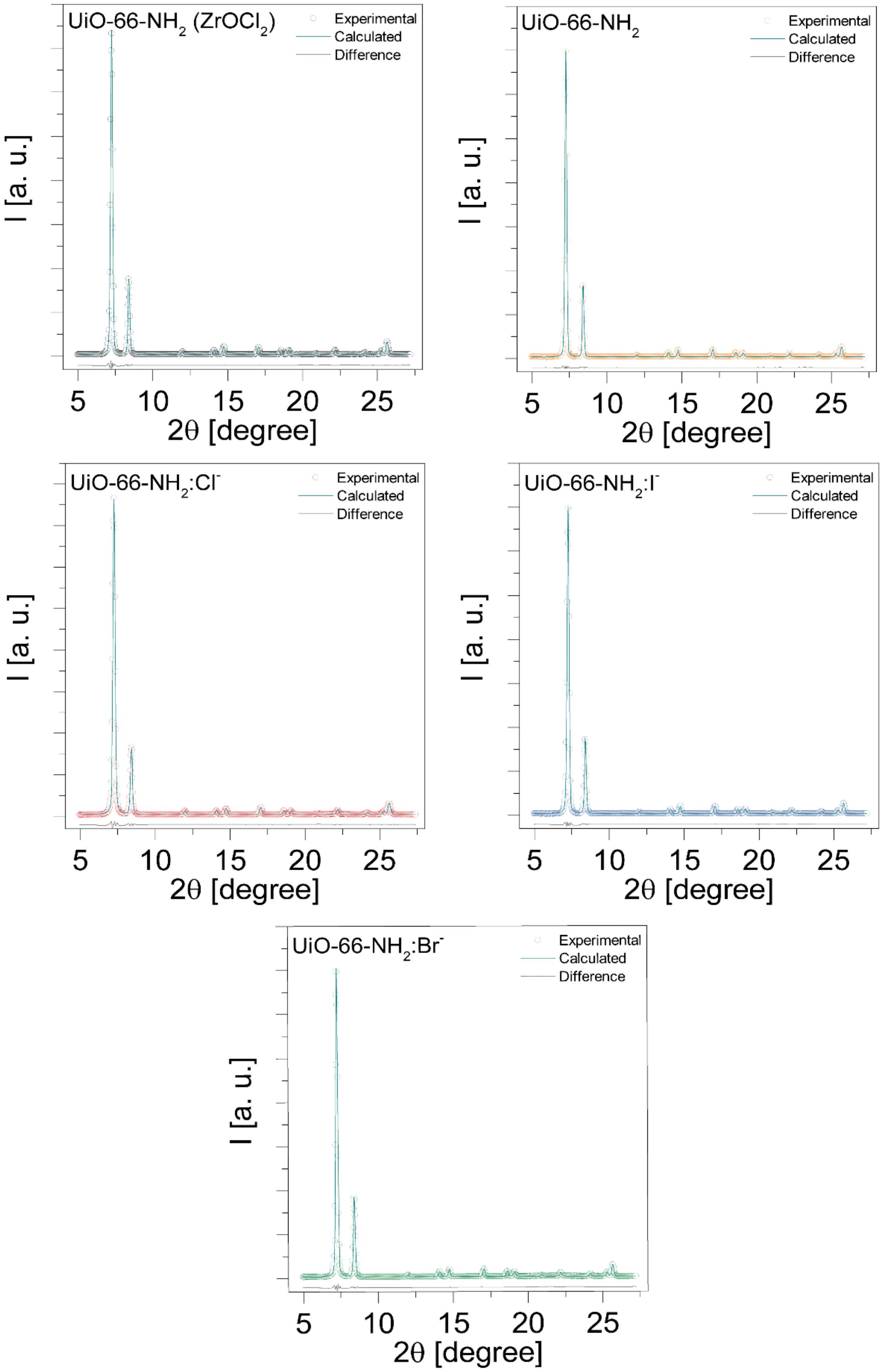

Figure S11: WAXS experiments measured at a sample to detector distance of 288 mm refined with Pawley's method and with corrected intensities and normalized with the most intense peak and residual.

Sample	a (Å)	V (Å³)
Reference[2]	20.77	8957.44
UiO-66-NH$_2$	20.81	9014.89
UiO-66-NH$_2$ (ZrOCl$_2$)	20.83	9036.86
UiO-66-NH$_2$:Cl$^-$	20.83	9044.03
UiO-66-NH$_2$:Br$^-$	20.82	9025.94
UiO-66-NH$_2$:I$^-$	20.82	9029.97

Table S2. Cell parameters obtained with Pawley's method.

RAMAN spectroscopy

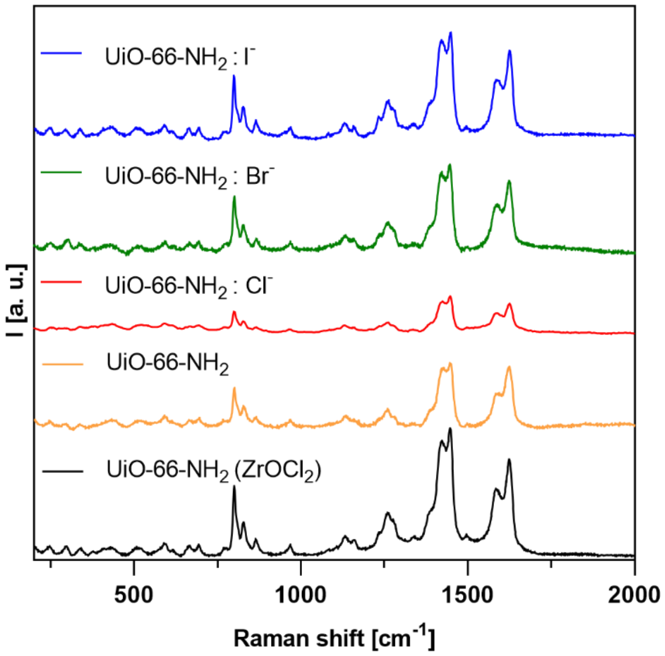

Figure S12. Raman spectra of UiO-66-NH$_2$ NMOFs.

TGA

TGA measurements were carried out in the presence of air, leading to the following degradation reaction:

$$\mathrm{Zr_6O_6-(C_8H_3O_4)_6-(NH_2)_{6(s)}+\frac{93}{2}O_{2(g)} \rightarrow\ 6ZrO_{2(s)}+48CO_{2(g)}+15H_{2(g)}+3N_{2(g)}}\quad (1)$$

For the TGA result representation, we consider the method described by Greig *at a*l.[3] in which the inorganic residue is related to the initial expected ideal molar mass of the Zr-cluster. Therefore, in our case, the molar mass of $Zr_6O_6(BDC)_6$-$(NH_2)_6$ is 1717.34 g mol^{-1}, a factor of 2.322 higher than the molar mass of the corresponding residue of 6 moles of ZrO_2 (6 x 123.22 = 739.34 g mol^{-1}). The end weight at 800 °C of a TGA run on UiO-66-NH$_2$ samples is normalized to 100 %, then the TGA plateau (solvent free, and dehydroxylated MOF) should ideally be found at 232.2 % as shown in Figure 5a. If the plateau of the experimental TGA falls of this theoretical weight that indicates that the NMOFs are lighter than that ideal formula and therefore, the UiO-66-NH_2 will be linker deficient.

Inductively Coupled Plasma Optical Emission Spectroscopy (ICP-OES)

ICP-OES analysis was performed to determine the final concentration and composition of the NPs after the synthesis. 20 µL of all the samples were digested overnight with 480 µL of aqua regia. Samples were diluted with 4.5 mL of HCl 2% v/v. The concentration in ppm (mg/L) of Zr and the yield of the reaction are presented in Table S3.

Sample	mg/mL Zr ICP	Yield of reaction (%)
UiO-66-NH_2 ($ZrOCl_2$)	0.21 ± 0.02	10.3 ± 0.98
UiO-66-NH_2	0.92 ± 0.03	34.1 ± 1.11
UiO-66-NH_2: Cl^-	2.08 ± 0.07	77.2 ± 2.60
UiO-66-NH_2: I^-	1.40 ± 0.34	44.9 ± 10.9
UiO-66-NH_2: Br^-	1.21 ± 0.27	51.9 ± 11.6

Table S3. ICP-OES results.

Using the reported data of the volume of the unit cell of the UiO-66-NH_2 and both the values of the Zr concentration obtained by ICP-OES (mg Zr/mL) and the volume of the NMOFs calculated from the SEM images, the molarity of the NMOFs can be easily calculated using the following equations (Table S4). The NMOFs were considered perfectly octahedral, and the following data was applied: no. (Zr) per unit cell=24; MW(Zr) = 91.2 g/mol.

$$\frac{unit\ cell}{UiO\ NMOF} = \frac{V_{UiO}}{V_{unit\ cell}}$$

Number of Zr atoms per UiO NMOFs was calculated using the number of Zr atoms per unit cell:

$$\frac{no.\ Zr\ atoms}{UiO\ NMOF} = 24 * \frac{unit\ cells}{UiO\ NMOF}$$

Using the molar weight of the Zr, the mg of Zr per UiO NMOF can be calculated as:

$$\frac{mg\ Zr}{UiO\ NMOF} = \frac{no. Zr\ atoms}{UiO\ NMOF} * \frac{1\ mol\ Zr}{N_A\ \ Zr} * \frac{91.2\ g\ Zr}{1\ mol\ Zr} * \frac{1000\ mg}{1g}$$

Finally, using the ICP-OES values (mg Zr/mL) and the mg Zr/UiO particle, we can calculate the molarity of the UiO:

$$\frac{UiO\ NMOF}{mL} = \frac{mg\ Zr}{mL} * \frac{UiO\ NMOF}{mg\ Zr}$$

$$concentration\ (nM) = \frac{UiO\ NMOF}{mL} * \frac{1\ mol\ UiO}{N_A\ UiO\ NMOF} * \frac{1000\ mL}{1\ L} * 10^9$$

	V SEM (nm^3)	unit cells/UiO	Zr/part UiO	mg Zr/UiO	UiO NPs/mL	nM UiO
UiO-66-NH_2 ($ZrOCl_2$)	1.04×10^6	1.16×10^5	2.78×10^6	4.22×10^{-13}	4.93×10^{11}	0.82
UiO-66-NH_2: Cl^-	3.92×10^5	4.38×10^4	1.05×10^6	1.59×10^{-13}	1.30×10^{13}	21.64
UiO-66-NH_2: Br^-	6.10×10^5	6.84×10^4	1.64×10^6	2.48×10^{-13}	5.63×10^{12}	9.34
UiO-66-NH_2: I^-	2.51×10^5	2.81×10^4	6.73×10^5	1.02×10^{-13}	1.19×10^{13}	19.70

Table S4. Concentration results, using the size (SEM) and ICP values, expressed in mg Zr/UiO and in nM.

In the particular case of the $ZrO(NO_3)_2$ the molarity could not be calculated due to the lack of a defined structure that enables to calculate the volume of each particle.

Dynamic Light Scattering analysis

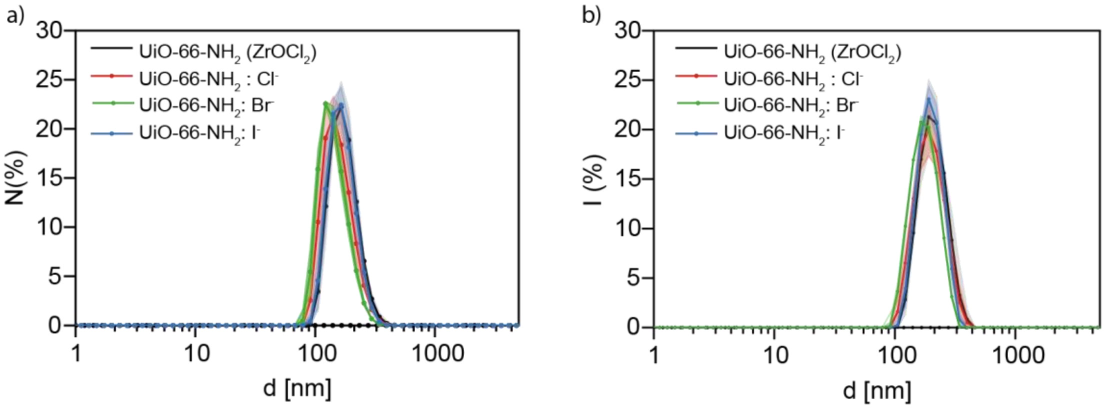

Figure S13. DLS intensity, volume, and number distributions of the hydrodynamic diameter d_h of the UiO-66-NH_2 samples.

Sample	**d_{SEM} (nm)**	**$d_{h,NTA}$ (nm)**	**$d_{h,N(DLS)}$(nm)**	**PDI**	**ζ (mV)**
UiO-66-NH_2 ($ZrOCl_2$)	225 ± 36	200 ± 3	202 ± 3	0.170	5.40 ± 0.1
UiO-66-NH_2	-	-	756 ± 74	0.483	-
UiO-66-NH_2: Cl^-	94 ± 10	140 ± 2	163 ± 5	0.040	8.70 ± 0.3
UiO-66-NH_2: Br^-	109 ± 14	136 ± 2	153 ± 5	0.030	16.0 ± 1.0
UiO-66-NH_2: I^-	81 ± 9	123 ± 1	167 ± 1	0.004	16.1 ± 0.4

Table S5. Size values of the UiO-66-NH_2 samples: Edge size (a) of the octahedral nanoparticles calculated using SEM images, hydrodynamic diameters d_h (mean value ± SD) as derived from DLS measurements and ζ- potential values (ζ ± SD). SD values correspond to the standard deviation of value as obtained from several repetitions (n=3) of the measurement. The polydispersity index (PDI) for each sample is also given.

S3. Colloidal stability in biologically relevant media

Mean values (± SD) are listed in Table S6.

Water				
t (h)	UiO-66-NH$_2$ (ZrOCl$_2$)	UiO-66-NH$_2$:Cl$^-$	UiO-66-NH$_2$:Br$^-$	Ui-66-NH$_2$:I$^-$
0	176 ± 10	158 ± 6	145 ± 4	169 ± 7
1	181 ± 8	169 ± 11	148 ± 15	170 ± 6
5	181 ± 7	165 ± 4	142 ± 6	160 ± 4
24	173 ± 10	159 ± 5	158 ± 4	167 ± 11
Lysosomal medium (PSF)				
t (h)	UiO-66-NH$_2$ (ZrOCl$_2$)	UiO-66-NH$_2$:Cl$^-$	UiO-66-NH$_2$:Br$^-$	UiO-66-NH$_2$:I$^-$
0	214 ± 10	173 ± 10	165 ± 10	185 ± 8
1	212 ± 9	189 ± 4	174 ± 2	175 ± 10
5	220 ± 11	191 ± 10	197 ± 14	204 ± 7
24	227 ± 47	200 ± 7	223 ± 26	200 ± 69
DMEM (completo)				
t (h)	UiO-66-NH$_2$ (ZrOCl$_2$)	UiO-66-NH$_2$:Cl$^-$	UiO-66-NH$_2$:Br$^-$	UiO-66-NH$_2$:I$^-$
0	196 ± 6	253 ± 10	201 ± 10	236 ± 8
1	247 ± 116	222 ± 21	220 ± 5	224 ± 2
5	251 ± 160	271 ± 10	221 ± 13	236 ± 20
24	245 ± 173	251 ± 100	201 ± 10	237 ± 9
PBS				
t (h)	UiO-66-NH$_2$ (ZrOCl$_2$)	UiO-66-NH$_2$:Cl$^-$	UiO-66-NH$_2$:Br$^-$	UiO-66-NH$_2$:I$^-$
0	212 ± 65	170 ± 10	180 ± 1	177 ± 11
1	292 ± 10	180 ± 13	212 ± 16	183 ± 4
5	312 ± 88	207 ± 14	183 ± 15	223 ± 14
24	668 ± 173	256 ± 42	250 ± 40	239 ± 20

Table S6. Hydrodynamic diameters d_h (mean value ± SD) as derived from DLS measurements of the NMOFs in the different media (water, PSF, DMEM and PBS) at different times (t=0,1,5 and 24h).

S4. UiO-66 NMOFs characterization

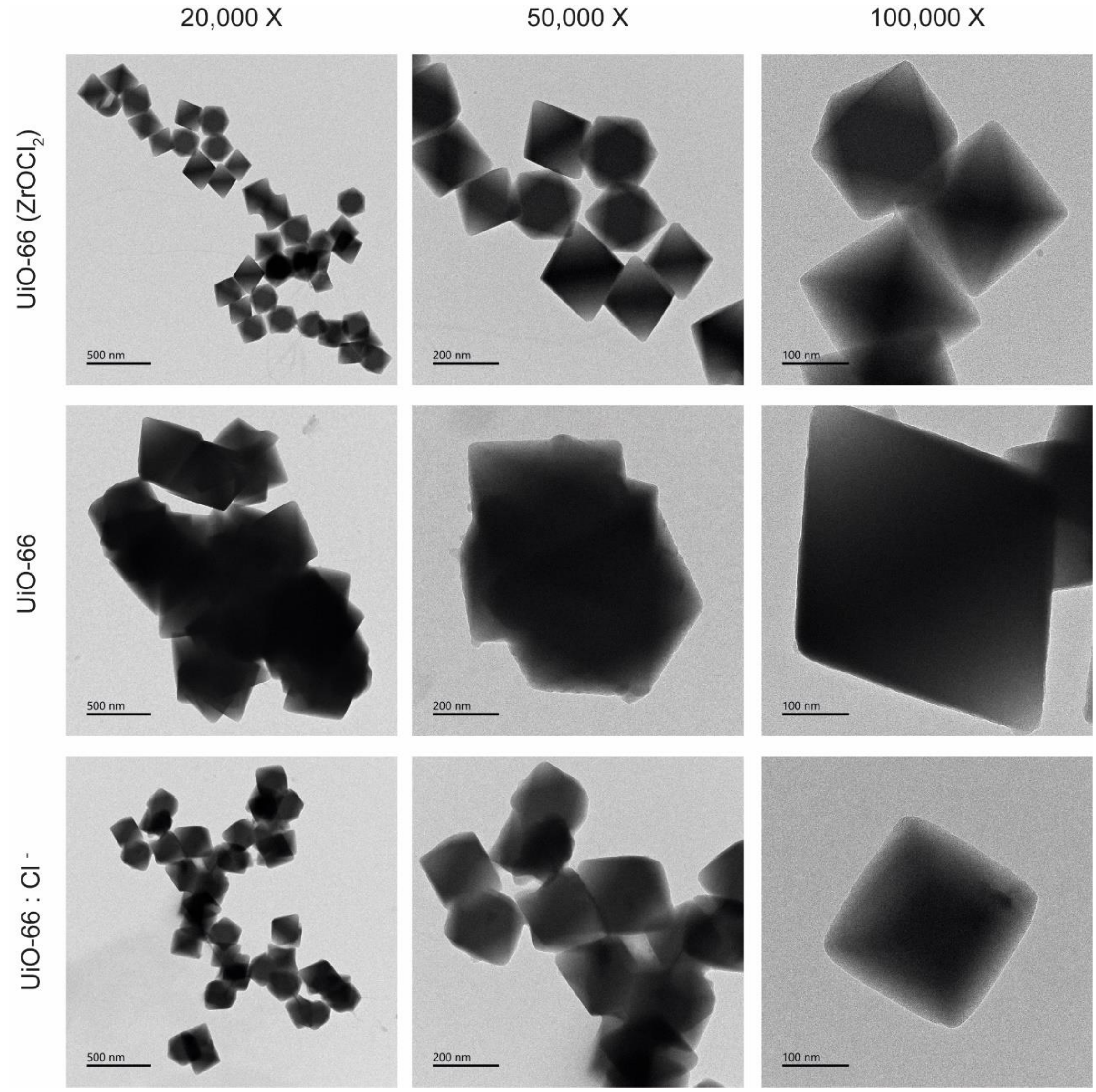

Figure S14. Representative TEM images of the UiO-66 nanoparticles synthesized with different Zr precursors and the effect of Cl$^-$ when the synthesis is performed with ZrO(NO$_3$)$_2$ precursor at different magnifications.

Sample	mg/mL Zr ICP	Yield of reaction (%)
UiO-66 (ZrOCl$_2$)	1.15	39.83
UiO-66	0.24	11.13
UiO-66: Cl$^-$	0.42	19.71

Table S7. ICP-OES results for UiO-66.

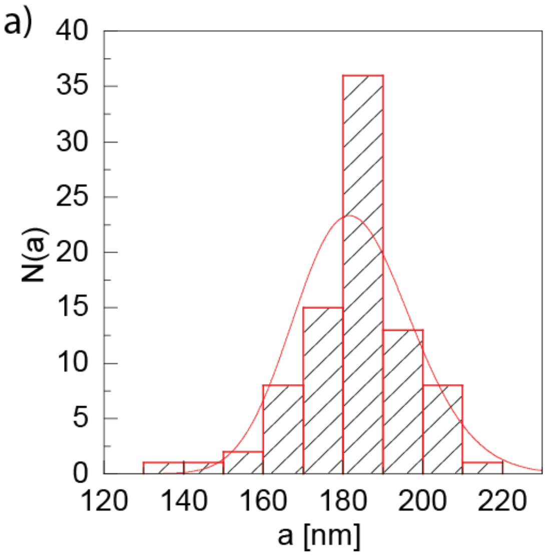

Figure S15. Histogram of the number distribution N of the edge of the NMOFs (i.e., vertex-to vertex distance) as determined from SEM images. a) UiO-66 ($ZrOCl_2$) 186 ± 13 nm and b) UiO-66:Cl^- 174 ± 13 nm.

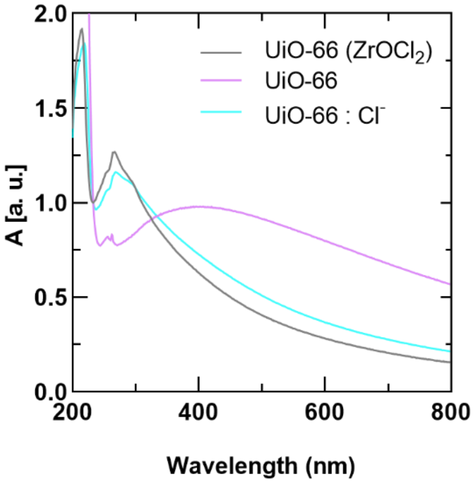

Figure S16. UV-VIS absorption spectra of the UiO-66 samples with different Zr precursors and the effect of Cl^- when the synthesis is performed with $ZrO(NO_3)_2$.

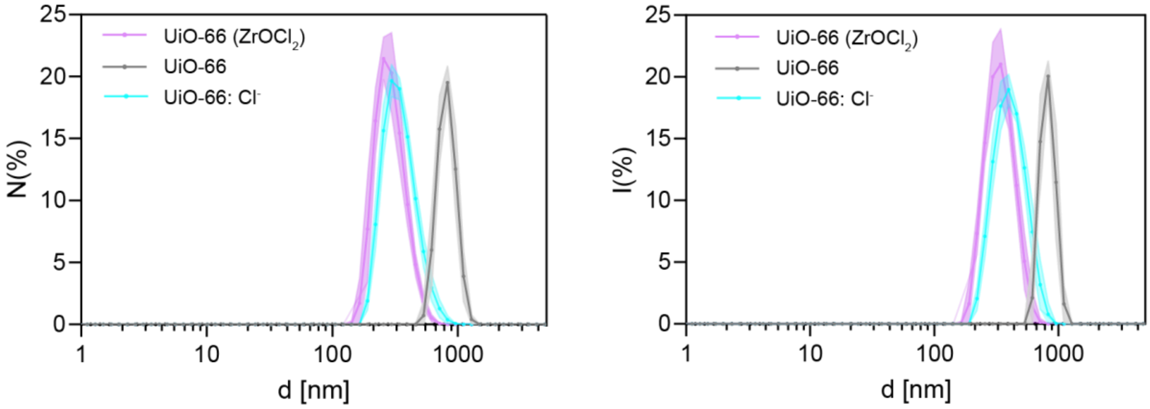

Figure S17. DLS a) number and b) intensity distributions of the hydrodynamic diameter d_h of the UiO-66 samples.

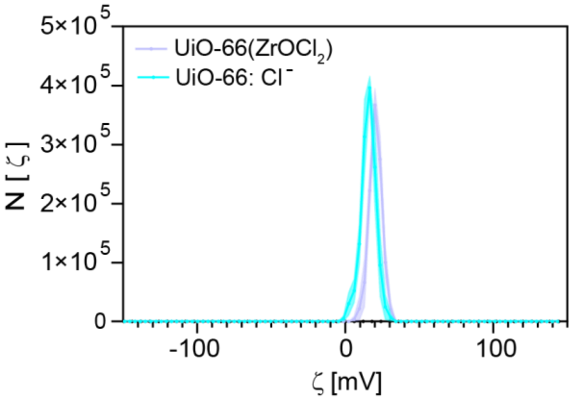

Figure S18. ζ-potential values for the UiO-66 samples

Sample	d_{SEM} (nm)	$d_{h,N(DLS)}$ (nm)	PDI	ζ (mV)
UiO-66 (ZrOCl$_2$)	186 ± 13	273 ± 82	0.072	26.4 ± 0.3
UiO-66	-	821 ± 42	0.414	4.8 ± 0.6
UiO-66: Cl$^-$	174 ± 13	376 ± 120	0.142	16.0 ± 0.3

Table S8. Size values of the UiO-66 samples: Edge size (a) of the octahedral nanoparticles calculated using SEM images, hydrodynamic diameters d_h (mean value ± SD) as derived from DLS measurements and ζ- potential values (ζ ± SD). The polydispersity index (PDI) for each sample is also given.

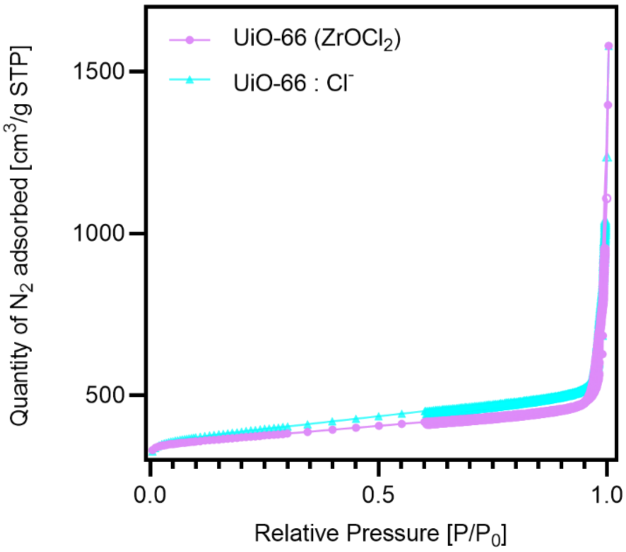

Figure S19. BET isotherm of UiO-66 (ZrOCl$_2$) and UiO-66:Cl$^-$.

S5. Rhodamine 6G loading

Table S9 summarizes some properties of Rhodamine 6G such as the molecular weight (MW), the excitation and emission wavelength and its size. R6G structure is shown in Figure S20.

Dye	MW (g/mol)	λ_{exc} (nm)	λ_{em} (nm)	Size (nm)
R6G	479.02	520	550/560	1.61

Table S9. Rhodamine 6G characteristics.

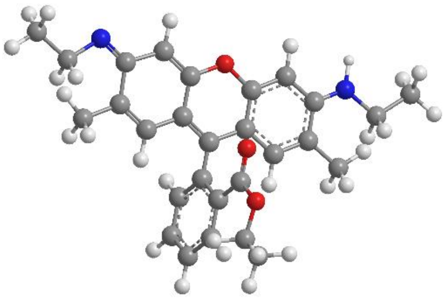

Figure S20. Rhodamine 6G molecule (Chem & Bio Draw 12.0)

Table S10 summarizes the conditions for the R6G loading.

Dye	[dye] (mg/mL)	[UiO] (mg/mL)	V_{R6G} (µL)	V_{UIO} (µL)	solvent
R6G	2	1	100	100	water

Table S10. Dye loading quantities.

Quantification by fluorescence measurements: Fluorescence characterization in solution was performed using an Infinite® 200 PRO, Tecan, Switzerland. The amount of R6G molecules loaded into the UiO-66-NH_2 as dispersed in water was quantified indirectly, by measuring the R6G fluorescence (λ_{ex}/ λ_{em} =520/560 nm) remaining in the supernatants after centrifugation and washing the NMOFs. The R6G concentration in the supernatant was determined by interpolation of the measured fluorescence intensity (I) to a previously constructed analytical calibration curve (Figure S21). This led to a value of R6G per NMOF presented in Table S11.

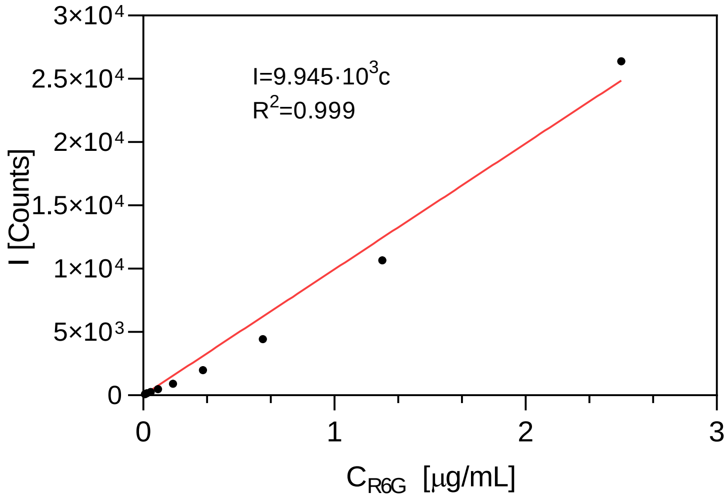

Figure S21. Calibration curve of R6G in water was obtained from fluorescence under excitation at 520 nm (I). Fluorescence intensity (I) at the maximum emission peak as a function of R6G concentration c is plotted and calibration equation is obtained by fitting a linear regression line to the collected data; R^2 is the coefficient of determination.

S6. UiO-66-NH$_2$:X$^-$@R6G NMOFs characterization

The results obtained are presented in Table S12, where the notation of @R6G has been added to all the samples to indicate they have been loaded. In the particular case of the UiO-66-NH$_2$@*R6G (*$ZrO(NO_3)_2$) the number of dye molecules per MOF could not be calculated due to the lack of a value of the molarity of the sample.

Figure S22. From left to right: UiO-66-NH$_2$: Br$^-$, UiO-66-NH$_2$: I$^{-,}$ UiO-66-NH$_2$: Cl$^-$, UiO-66-NH$_2$ ($ZrOCl_2$), UiO-66-NH$_2$.

Sample	% R6G IN	R6G/MOF	mg R6G/mgZr	mol R6G/mgZr	w/w (%)
UiO-66-NH$_2$@*R6G* *(*$ZrOCl_2$)	28%	2.97×10^5	0.56	2.34×10^{-7}	17.5
UiO-66-NH$_2$@*R6G*	21%	-	0.42	1.75×10^{-7}	-
UiO-66-NH$_2$: Cl$^-$ @*R6G*	28%	1.12×10^5	0.56	2.34×10^{-7}	17.5
UiO-66-NH$_2$: Br$^-$ @*R6G*	31%	1.94×10^5	0.62	2.59×10^{-7}	19.4
UiO-66-NH$_2$: I$^-$ @*R6G*	27%	6.92×10^5	0.54	2.25×10^{-7}	16.9

Table S11. Dye loading for the UiO-66-NH$_2$ nanoparticles. Percentage of the maximum dye loaded in the nanoparticles calculated via fluorescence measurements of the supernatant, number of dye molecules per UiO NP and dye molecules/dye mg per mg of Zirconium.

UV-Vis spectroscopy: A Biochrom Libra S60 UV-Vis spectrophotometer was used to record UV-Vis absorption spectrum of the samples in water after the R6G encapsulation (Figure S23). The spectra show a significant absorption peak was observed (at 550 nm).

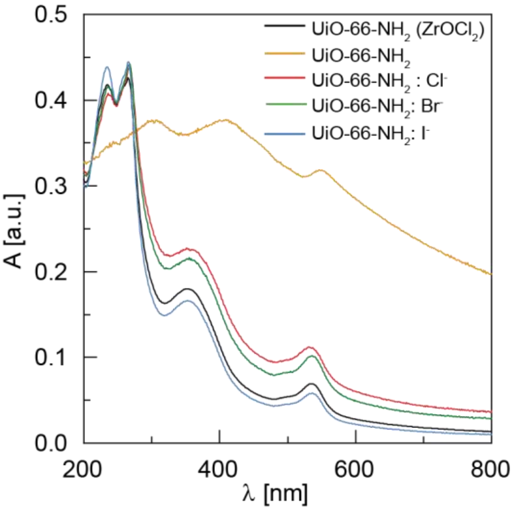

Figure S23. UV-Vis absorption spectra normalized to Zr of the UiO-66-NH$_2$ NMOFs after the R6G loading.

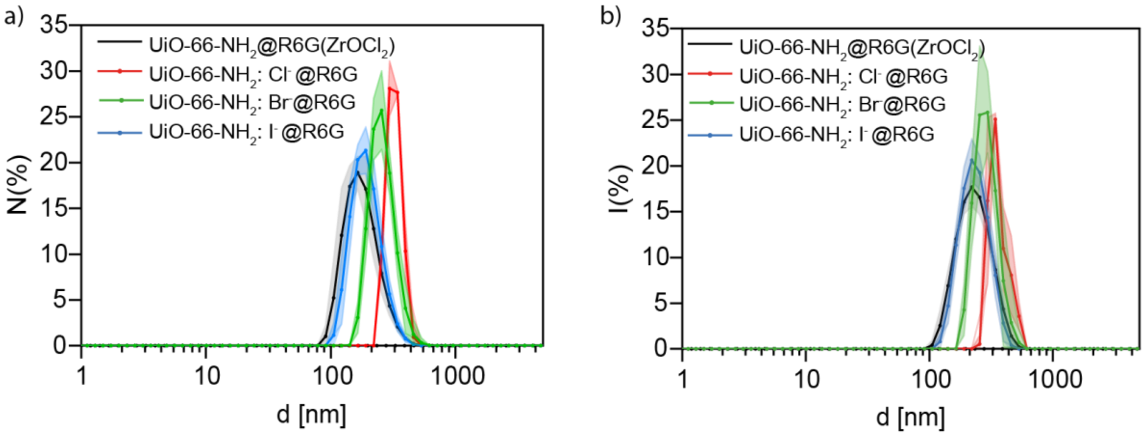

Figure S24. DLS a) intensity and b) number distributions of the hydrodynamic diameter d_h of the UiO-66-NH$_2$@R6G NMOFs.

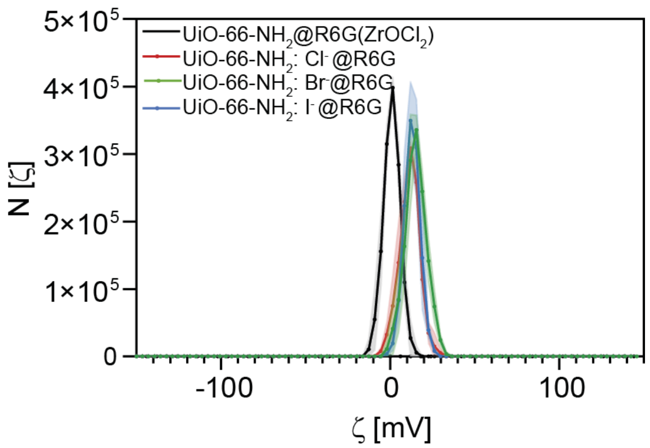

Figure S25. ζ- potential distribution for the UiO-66-NH$_2$ samples after the R6G loading.

Sample	**$d_{h,N}$ (nm)**	**$d_{h,I}$ (nm)**	**PDI**	**ζ (mV)**
UiO-66-NH$_2$@*R6G* (ZrOCl$_2$)	182 ± 12	238 ± 7	0.12	-0.3 ± 0.1
UiO-66-NH$_2$:Cl$^-$@*R6G*	271 ± 80	319 ± 76	0.86	13.4 ± 0.5
UiO-66-NH$_2$:Br$^-$@*R6G*	254 ± 11	290 ± 25	0.32	15.8 ± 0.1
UiO-66-NH$_2$:I$^-$@*R6G*	192 ± 5	237 ± 10	0.23	15.7 ± 0.3

Table S12. Hydrodynamic diameters d_h (mean value ± SD) as derived from DLS measurements of the UiO-66NH$_2$ samples as dispersed in water after the dye loading. The polydispersity index (PDI) and ζ potential for each sample is also given.

S7. UiO-66@R6G MOFs characterization

The encapsulation was repeated for the UiO-66 samples using the same conditions used for UiO-66-NH_2. The results are shown in Table S13.

Sample	% R6G IN	R6G/MOF	mg R6G/mgZr	mol R6G/mgZr	w/w (%)
UiO-66@ *R6G* ($ZrOCl_2$)	30%	6.15×10^5	0.60	2.51×10^{-7}	18.7
UiO-66 @*R6G*	20%	-	0.40	1.67×10^{-7}	-
UiO-66: Cl^- @*R6G*	29%	7.50×10^5	0.58	2.42×10^{-7}	18.1

Table S13. Dye loading for the UiO-66 NMOFs. Percentage of the maximum dye loaded in the nanoparticles calculated via fluorescence measurements of the supernatant, number of dye molecules per UiO NP and dye molecules/dye mg per mg of Zirconium.

Again, in the table there is a missing value corresponding to the mol dye/MOF due to the lack of a defined structure of the UiO-66 synthesized without the Cl^-.

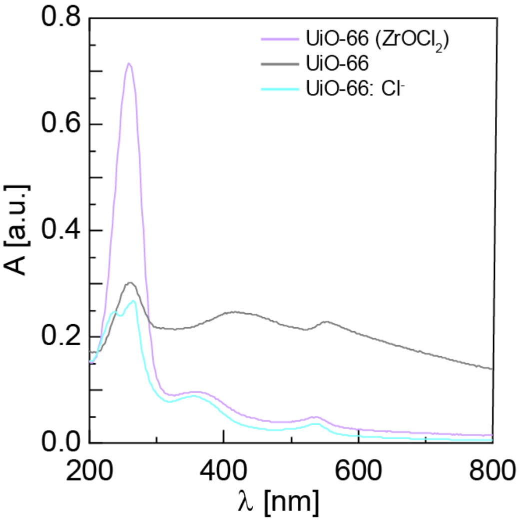

Figure S26. UV-VIS absorption spectra normalized to Zr (λ=212 nm) of the UiO-66 samples after the R6G loading.

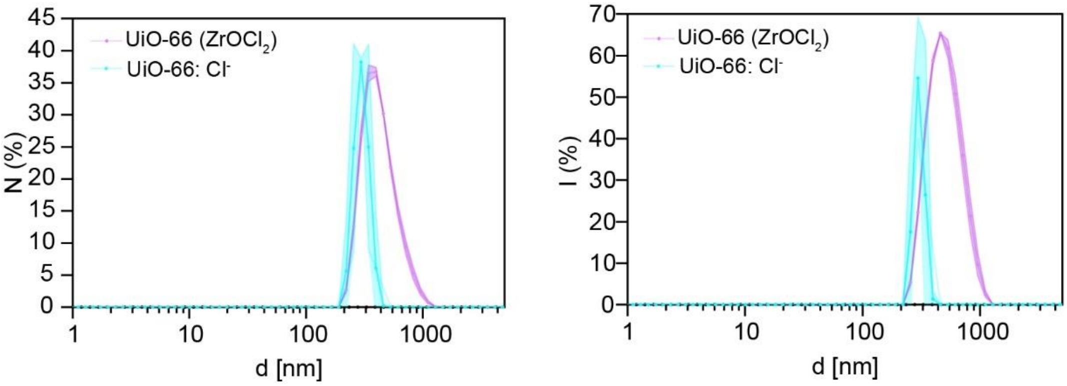

Figure S27. DLS a) intensity and b) number distributions of the hydrodynamic diameter d_h of the UiO-66 @R6G NMOFs.

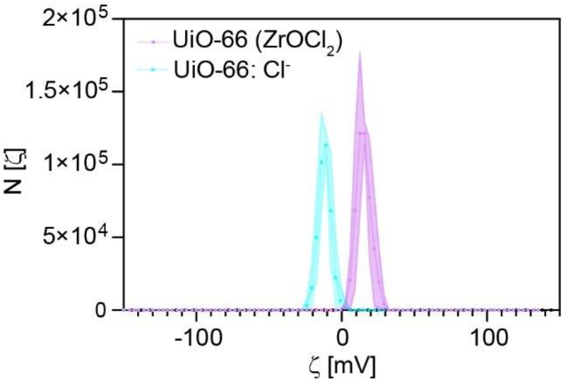

Figure S28. ζ- potential distribution for the UiO-66 samples after the R6G loading.

Sample	$d_{h,N}$ (nm)	$d_{h,I}$ (nm)	**PDI**	**ζ (mV)**
UiO-66@*R6G* ($ZrOCl_2$)	438 ± 20	790 ± 140	0.51	-15.1 ± 0.3
UiO-66: Cl^- @*R6G*	299 ± 29	302 ± 29	0.32	-7.7 ± 0.4

Table S14. Hydrodynamic diameters d_h (mean value ± SD) as derived from DLS measurements of the UiO-66 samples as dispersed in water after the dye loading. The polydispersity index (PDI) and ζ potential for each sample is also given.

S8. Cargo loading stability in biologically relevant media

Cargo loading stability: At each time point, 100 µL of these samples were centrifuged to remove the supernatant (SN) and measure its fluorescence using the same procedure that was used previously to calculate the dyes/MOF. In this case, the concentration of free R6G in the supernatant was determined by interpolation of the measured fluorescence intensity (I) to the previously constructed analytical calibration curve in water and new calibration curves in DMEM and PSF (Figure S29). The results are presented in Table S15 for UiO-66-NH$_2$ and Table S16 for the UiO-66.

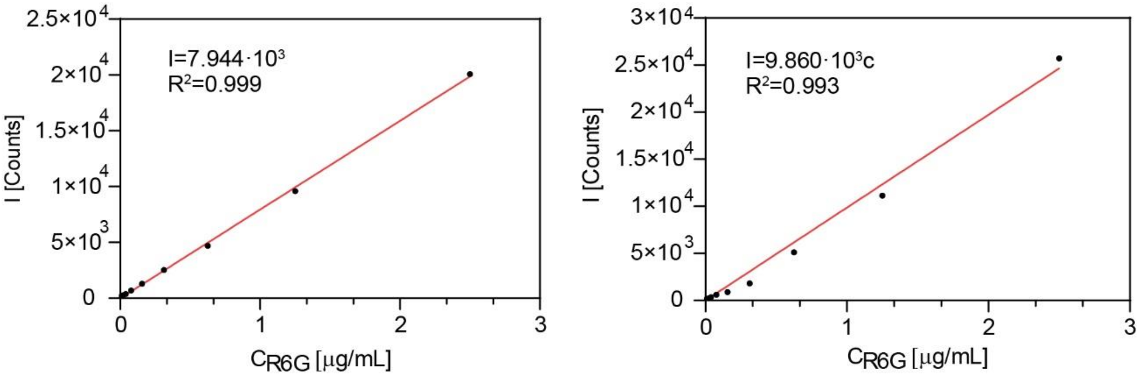

Figure S29. Calibration curves of R6G in PSF and DMEM

		WATER (% SN)			
t (h)	*UiO-66-NH$_2$ (ZrOCl$_2$)*	*UiO-66-NH$_2$*	*UiO-66-NH$_2$:Cl$^-$*	*UiO-66-NH$_2$:Br$^-$*	*UiO-66-NH$_2$:I$^-$*
0	0.08%	0.20%	0.22%	0.31%	0.03%
1	0.34%	0.28%	0.57%	0.75%	0.09%
5	0.50%	0.23%	0.81%	1.35%	0.17%
24	0.65%	0.35%	1.07%	1.77%	0.26%
		PSF (% SN)			
t (h)	*UiO-66-NH$_2$ (ZrOCl$_2$)*	*UiO-66-NH$_2$*	*UiO-66-NH$_2$:Cl$^-$*	*UiO-66-NH$_2$:Br$^-$*	*UiO-66-NH$_2$:I$^-$*
0	0.39%	0.22%	0.78%	0.94%	0.18%
1	0.37%	0.33%	1.19%	1.74%	0.25%
5	0.92%	0.49%	1.80%	2.30%	0.49%
24	1.47%	0.88%	2.94%	3.14%	1.19%
		DMEM (% SN)			
t (h)	*UiO-66-NH$_2$ (ZrOCl$_2$)*	*UiO-66-NH$_2$*	*UiO-66-NH$_2$:Cl$^-$*	*UiO-66-NH$_2$:Br$^-$*	*UiO-66-NH$_2$:I$^-$*
0	0.79%	0.47%	1.37%	1.39%	0.27%
1	0.31%	0.52%	1.74%	2.17%	0.54%
5	2.14%	0.84%	2.69%	1.40%	1.06%
24	1.33%	1.16%	3.84%	4.48%	2.72%

Table S15. R6G released from the pores of the nanoparticles.

WATER (% SN)			
t (h)	UiO-66 ($ZrOCl_2$)	UiO-66	UiO-66:Cl^-
0	0.11%	0.28%	0.51%
1	0.17%	0.35%	1.00%
5	0.18%	0.55%	1.69%
24	0.67%	0.77%	1.82%
PSF (% SN)			
t (h)	UiO-66 ($ZrOCl_2$)	UiO-66	UiO-66:Cl^-
0	0.48%	1.00%	1.27%
1	0.94%	1.42%	2.04%
5	4.89%	6.64%	6.87%
24	6.69%	7.85%	10.75%
DMEM (% SN)			
t (h)	UiO-66 ($ZrOCl_2$)	UiO-66	UiO-66:Cl^-
0	1.00%	1.58%	2.76%
1	1.57%	2.00%	3.66%
5	2.99%	1.01%	4.17%
24	4.01%	2.63%	7.25%

Table S16. R6G released from the pores of the nanoparticles at times t=0.1.5 24 and 48h.

S9. Cell studies

Cell toxicity

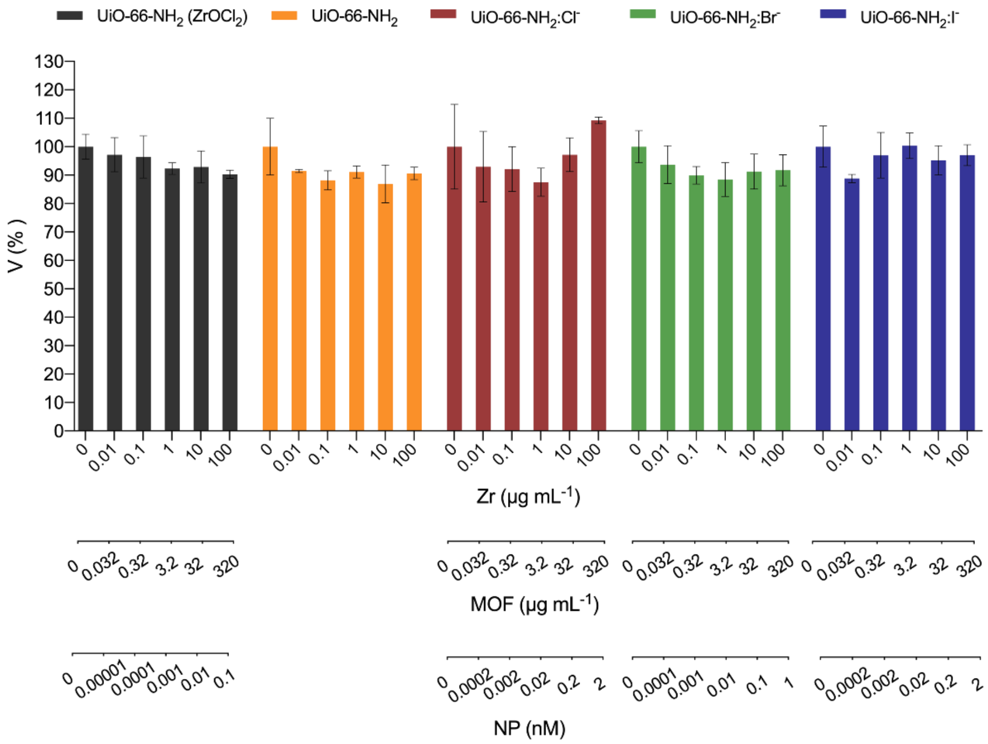

Figure S30. Cell viability in A549 cell culture after 24 h of UiO-66-NH$_2$ NMOFs exposure, measured by Resazurin assay. Viability values represents the mean ± standard deviation of measurements from three different wells. X axes representing the NMOF concentration in terms of Zr, NMOF and NP concentration unless in UiO-66-NH$_2$ where the lack of a defined structure prevents the calculation of the volume of each particle.

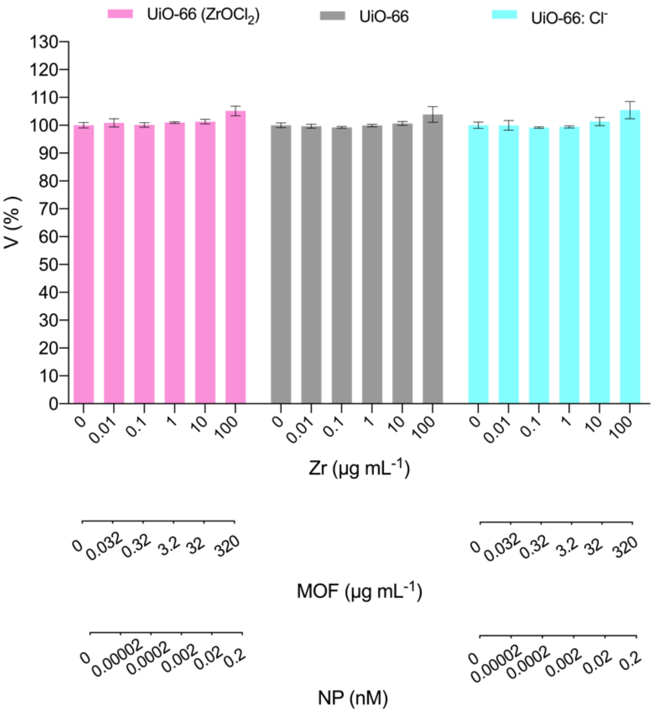

Figure S31. Cell viability in A549 cell culture after 24 h of UiO-66 NMOFs exposure, measured by Resazurin assay. Viability values represents the mean ± standard deviation of measurements from three different wells.

Cellular Uptake

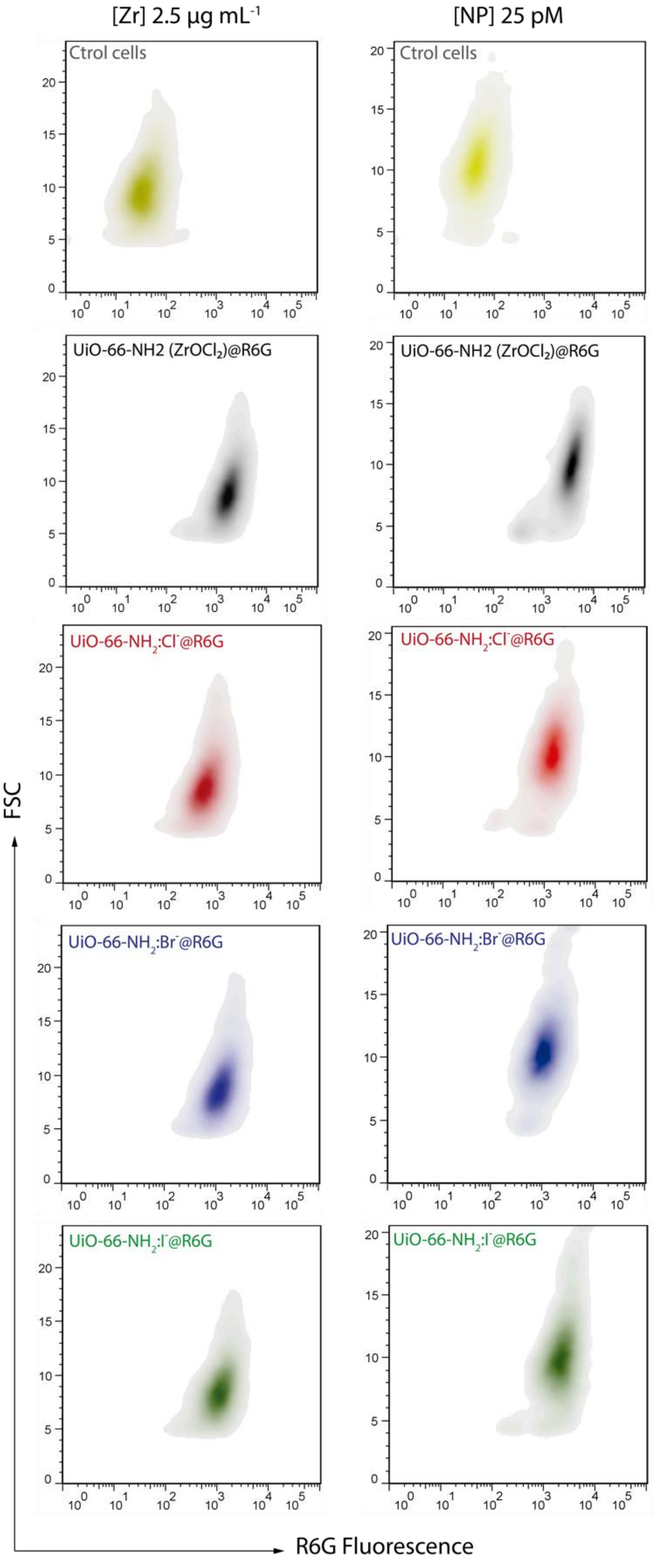

Figure S32. UiO-66 cell uptake assessment by flow cytometry. Dot plots indicating the cells distribution as function of the rhodamine 6G fluorescence. Each plot represents the measurement of at least 5000 events.

	[Zr] (µg/mL)	MFI	[R6G] (µg/mL)	corrected MFI
UiO-66-NH_2($ZrOCL_2$)@R6G	2.5	1778.66± 17.61	1.65	1778.66 ± 17.61
UiO-66-NH_2:Cl^-@R6G	2.5	649.66 ± 9.29	1.1	864.05 ± 12.35
UiO-66-NH_2:Br^-@R6G	2.5	1214.33 ± 9.45	1.1	1615.06 ± 12.57
UiO-66-NH_2:I^-@R6G	2.5	1311.33 ± 11.23	1.25	1639.16 ± 14.04

Table S17. Flow cytometry measurements of UiO-66 uptake by A549 cells. Mean fluorescence intensity (MFI) of experiment using an incubation with a constant concentration of Zr (2.5 µg/mL) and the corrected value normalized to the R6G content for each NMOF.

S10. References

1. D. B. Dwyer, D. T. Lee, S. Boyer, W. E. Bernier, G. N. Parsons and W. E. Jones, *ACS Appl. Mater. Interfaces*, 2018, **10**, 25794-25803.
2. Y. Ma, X. Han, S. Xu, Z. Wang, W. Li, I. da Silva, S. Chansai, D. Lee, Y. Zou, M. Nikiel, P. Manuel, A. M. Sheveleva, F. Tuna, E. J. L. McInnes, Y. Cheng, S. Rudić, A. J. Ramirez-Cuesta, S. J. Haigh, C. Hardacre, M. Schröder and S. Yang, *J. Am. Chem. Soc.*, 2021, **143**, 10977-10985.
3. G. C. Shearer, S. Chavan, S. Bordiga, S. Svelle, U. Olsbye and K. P. Lillerud, *Chem. Mater.*, 2016, **28**, 3749-3761.